Morning Transition of the Boundary Layer over Dallas–Fort Worth

KIP F. NIELSEN[a] AND DAVID A. RAHN[a]

[a] *Department of Geography and Atmospheric Science, University of Kansas, Lawrence, Kansas*

(Manuscript received 26 August 2021, in final form 29 June 2022)

ABSTRACT: Temperature profiles of the lower atmosphere (<3 km) over complex urban areas are related to health risks, including heat stress and respiratory illness. This complexity leads to uncertainty in numerical simulations, and many studies call for more observations of the lower atmosphere over cities. Using 20 years of observations from the Aircraft Meteorological Data Relay (AMDAR) program over Dallas–Fort Worth, Texas, average profiles every 0.5 h are created from the 1.5 million individual soundings. Dallas–Fort Worth is ideal because it is a large urban area in the central Great Plains, has no major topographic or coastal influences, and has two major airports near the center of the urban heat island. With frequent and high-quality measurements over the city, we investigate the evolution of the lower atmosphere around sunrise to quantify the stability, boundary layer height, and duration of the morning transition when there are southerly winds, few clouds, and no precipitation so as to eliminate transient synoptic events. Characteristics of the lower atmosphere are separated by season and maximum wind speed because the the Great Plains low-level jet contributes to day-to-day variability. In all seasons, stronger wind over the city leads to a weaker nocturnal temperature inversion at sunrise and a shorter morning transition period, with the greatest difference during autumn and the smallest difference during summer. During summer, the boundary layer height at sunrise is higher on average, deepens the most as wind strengthens, and has the fewest days exhibiting a surface temperature inversion over the city.

SIGNIFICANCE STATEMENT: Cities impact health by creating an urban heat island caused by more heating at the surface, less evaporative cooling, and increased anthropogenic waste heat, and they can have high pollution. Cooling overnight stabilizes the lower atmosphere and traps pollutants near the surface until surface heating after sunrise mixes them away. Inadequate pollution observations make it difficult to study these issues. The greatest mixing occurs about 2 h after sunrise but can be modulated by wind speed. Observations from 1.5 million aircraft landing and taking off over Dallas–Fort Worth, Texas, reveal that strong low-level wind leads to morning transitions ending 0.84 h earlier on average than with light wind. Details from this vast dataset contribute to improved understanding of the lower atmosphere over cities and provide a baseline for simulations.

KEYWORDS: Boundary layer; Diurnal effects; Heat islands; Aircraft observations; Urban meteorology

1. Introduction

Urbanization replaces natural land cover with low-albedo impervious surfaces, drastically altering the local radiative balance and energy exchange by reducing evapotranspiration and increasing sensible heat flux (Oke 1988; Arnfield 2003). This results in higher land surface temperatures (Tran et al. 2006; Imhoff et al. 2010; Peng et al. 2011) and higher air temperatures (Oke 1995; Azevedo et al. 2016) when compared with the rural surroundings, known as the urban heat island (UHI; Oke 1982). The maximum intensity of the UHI typically occurs at night, and during the day urban areas can be slightly cooler than the rural surroundings (Hafner and Kidder 1999; Morris and Simmonds 2000; Unwin 1980; Myrup et al. 1993; Basara et al. 2008). The UHI and its connection to the mixed-layer depth and persistence are related to health risks including heat stress and respiratory illness linked to air pollution. Continued urbanization and anthropogenic global warming over the next several decades will threaten public health, so it is crucial to understand the characteristics and behavior of the atmosphere over the urban environment.

Much of the work tied to UHIs focuses on the radiometric surface temperature or 2-m air temperature, which is strongly connected to physical factors of the local built environment. An equally important issue is how the lower atmosphere (<3 km) above the urban area is modified. The temperature profile and the 2-m air temperature are both influenced by factors such as the amount of thermally or mechanically generated turbulence. Over cities, atmospheric processes can be heavily modified due to increased surface roughness and large changes of the surface and urban canopy energy balance when compared with rural environments. The exact relationships can be difficult to assess given the lack of observations, uncertainty of numerical simulations, and the large influence of external factors driven by the day-to-day meteorology such as cloud cover, static stability, wind speed, frontal passages, and other transient weather events.

A particular feature of the lower atmosphere that has broader impacts on public health is the maintenance of stable conditions near the surface in the morning that keeps pollution, especially pollution emitted by the high traffic during the morning commute, concentrated near the surface (e.g., Gupta and Elumalai 2019). The pollution often disperses over a deeper layer as the daytime surface heating destabilizes the lower atmosphere enough to overcome the low-level stability

Corresponding author: David A. Rahn, darahn@ku.edu

DOI: 10.1175/JAMC-D-21-0169.1

and begins a rapid increase of the mixed-layer depth. The time between sunrise and the onset of this rapid increase is defined as the morning transition (e.g., Halios and Barlow 2018) and a longer morning transition can be associated with higher amounts of pollution remaining near the surface for a longer time. Although pollution motivates the study, we note that there are insufficient long-term hourly surface pollution observations to directly assess this connection here and we focus on the characteristics of the lower atmosphere.

Many factors can lead to the seasonal and day-to-day variation in the morning transition duration since several mechanisms can influence the amount of mixing in the lower atmosphere over a city. The greater surface roughness over urban areas contributes to greater mechanically generated turbulence, but this factor changes little over the observational time period so it is not a cause of the day-to-day variability. On the other hand, wind shear can substantially alter the lower atmosphere by promoting more mixing near the surface, which can inhibit a strong surface radiation inversion from developing overnight. In addition to increased mechanical turbulence, the greater heat storage of urban areas is related to the characteristics of the built environment, which increases sensible heating overnight and can promote mixing from below. These factors can work together to create greater mixing near the surface and decreases the time until the rapid growth of the mixed layer occurs (Halios and Barlow 2018).

Besides the complexity of processes over a range of scales, dependence on the surface characteristics, and uncertainty inherent in numerically simulating the complex urban environment, there is also a lack of observations of the lower atmosphere over cities. More specifically, high-vertical-resolution profiles of temperature, humidity, and wind with much higher temporal density than provided by traditional operational sources like radiosondes. The lack of measurements is not an issue unique to cities, and a broad range of instrumentation is needed to address a diverse set of research questions (Helbig et al. 2021). Many studies specifically point out that the lack of observations over cities impedes progress (e.g., Chen et al. 2011; Duarte et al. 2012; Deppe et al. 2013; Banta et al. 2013; Helmis et al. 2013; Mahrt et al. 2014; Wei et al. 2014). Upper-air observations are difficult to obtain on a regular basis. Few urban areas are near operational radiosondes, which are launched only 2 times per day, and radiosonde launches over cities are limited by air traffic control. Mean profiles of temperature can be obtained from satellites (Hu and Brunsell 2015) but lack sufficient details of shallow layers near the surface, temporal sampling can be infrequent, and retrievals must account for additional factors such as surface emissivity and view angle issues. Ceilometers do not contain temperature and wind profiles but provide some information on the lower atmosphere through attenuated backscatter from clouds and aerosols to detect the cloud-base or mixed-layer height. However, aerosol-derived mixed-layer height may differ from turbulence-derived mixing-layer height and be more representative of past turbulence rather than the current conditions (Kotthaus et al. 2018).

The availability of profiles from commercial aircraft through the Aircraft Meteorological Data Relay (AMDAR) program offers an opportunity to advance understanding of the urban boundary layer (BL). Observations from AMDAR have steadily grown over the last couple of decades, and the number is likely to keep increasing, despite a temporary reduction due to fewer flights during the COVID-19 pandemic. Although the sampling of the lower atmosphere is tied to airports, the advantage of AMDAR is the high temporal frequency, good vertical resolution, and quality data (e.g., Petersen 2016; Zhang et al. 2019; Wagner and Petersen 2021; Williams et al. 2021).

Given the importance of temperature and wind speed profiles over cities and the noted lack of observations that have inhibited progress, there are three objectives: 1) assess the ability of AMDAR to depict the evolution of the lower atmosphere at half-hourly intervals over a city, 2) determine the climatological features of the lower atmosphere over an urban area including the end of the morning transition that marks the onset time of the rapid growth of the daytime BL, and 3) investigate the role of low-level winds in explaining the day-to-day variability of the lower atmosphere.

2. Data and methods

a. Study location and local climate factors

Given the objectives above, it is necessary to select a location within an UHI with many observations before and after sunrise that is minimally affected by non-UHI effects that can systematically affect the BL, including sea breezes and topographic effects. The Dallas–Fort Worth area in Texas has two major airports, Dallas–Fort Worth International Airport (DFW) and Dallas Love Field Airport (DAL). This is an ideal location because it is a large urban area, has a high volume of air traffic, DAL and DFW are both near the UHI core (Fig. 1), and the local weather is not impacted by any major topographic or coastal features. The area is also prone to heat waves and droughts that are associated with significant health and economic impacts.

The nocturnal low-level jet (LLJ) is a prominent feature over the Great Plains and can form after turbulent mixing near the surface decreases (Blackadar 1957; Shapiro and Fedorovich 2009). There is a lingering debate over the causes of the LLJ, but mechanisms that support its formation include an inertial oscillation (Blackadar 1957; Parish and Oolman 2010; Shibuya et al. 2014), baroclinicity associated with sloping terrain (Holton 1967), conservation of potential vorticity (Zhong et al. 1996), and large-scale meteorological forcing (Song et al. 2005; Hu et al. 2013). The Great Plains LLJ is still an active area of research after decades of investigation (e.g., Parish and Clark 2017; Jahn and Gallus 2018; Gebauer and Shapiro 2019; Smith et al. 2019).

As the LLJ intensifies, mechanically generated turbulence is enhanced by the increased wind shear underneath the local maximum of wind speed aloft, and the turbulence may be transported down toward the surface (Smedman et al. 1997; Mahrt 1999; Ha and Mahrt 2001; Mahrt and Vickers 2002; Lundquist and Mirocha 2008; Hu et al. 2013; Brunsell et al.

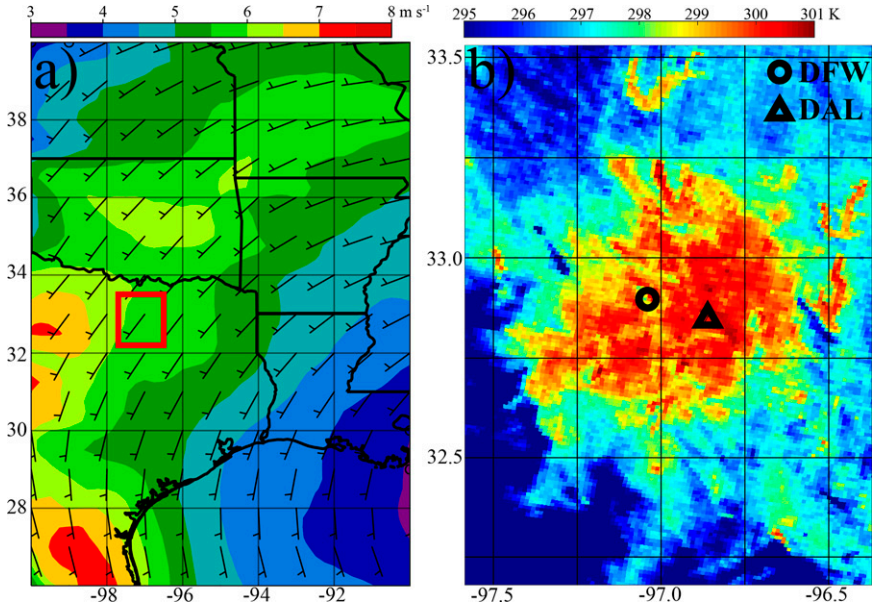

FIG. 1. (a) The 2001–20 average 1000 UTC 900-hPa wind speed (m s^{-1}) and wind barbs from ERA5 (Hersbach et al. 2020), and (b) land surface temperature (K) from *Aqua* MODIS (MYD11 L2) for Dallas–Fort Worth at 0810 UTC 19 Jun 2018 for the area outlined in red in (a), with the locations of DFW (circle) and DAL (triangle).

2021). The increase of turbulence is likely to have a large impact on the BL as it also interacts with the urban landscape. As the flow associated with the LLJ moves from rural areas to urban areas, the surface roughness increases and the surface energy balance shifts. These factors will modify the structure of the lower atmosphere over the surface of the city and downwind and have implications for both surface temperature and pollution dispersion over the city.

Although this study does not directly observe the surface layer, the surface layer is a critical zone for land–atmosphere interactions and changes drastically between rural and urban surfaces. The LLJ can have a substantial impact on the surface layer (e.g., Sun et al. 2012; Brunsell et al. 2021), and the impact should be even more pronounced as the flow moves over a city where the surface roughness is greater and the stability is lower because of greater sensible heat overnight relative to the rural surroundings. Turbulence regimes are related to the nocturnal LLJ and depend on the maximum wind speed and the shear below the LLJ (Mahrt and Vickers 2002; Banta et al. 2006). Bonin et al. (2015) also explored the idea of a threshold wind speed and found that wind speed above the surface (200 m) could be used to determine if turbulence is likely to be transported through a deeper layer. The magnitude of the LLJ can have a pronounced influence on the temperature profile over both rural and urban areas (Hu et al. 2013), and these regimes can play a critical role in modifying the near-surface characteristics including depth and evolution of the mixed layer.

b. *Treatment of AMDAR observations*

All AMDAR reports include static pressure, temperature, and wind, with some including water vapor and clear-air turbulence information (Petersen et al. 2016; Petersen 2016). Of the approximately 3500 aircraft that have atmospheric measurements, only 150 have moisture sensors (Williams et al. 2021). Although AMDAR observations are available to the National Weather Service in real time, data older than 48 h are available publicly on the Meteorological Assimilation Data Ingest System.

Care must be taken when processing the raw measurements since there is a vast amount of data and the reported height is the pressure altitude, which uses the static pressure measurement and the standard atmosphere to estimate the height. A better height estimate is obtained following the procedure in Rahn and Mitchell (2016) that uses measurements from the surface station at the airport and the aircraft with the hypsometric equation to estimate the actual, and not standard atmosphere, height. The data quality is high, but some issues have been noted such as a systematic warm bias of the AMDAR data when compared with radiosonde measurements (Ballish and Kumar 2008). The warm bias near the surface is only a few tenths of a degree but increases up to 1°C near 300 hPa. Since the focus of this project is on the lower part of the atmosphere, especially given the shallow BL during the morning, the larger biases aloft are not a concern.

This study used all AMDAR profiles collected between 2000 and 2020 at DFW (941 111 soundings) and DAL (636 254). Recent years tend to have more soundings than earlier years, with an exception during 2020 when air travel was substantially reduced. Aircraft observations are not uniformly distributed over all hours of the day since fewer flights arrive or depart in the middle of the night. However, there are still many soundings before sunrise, mainly because DFW is a hub for the United Parcel Service company.

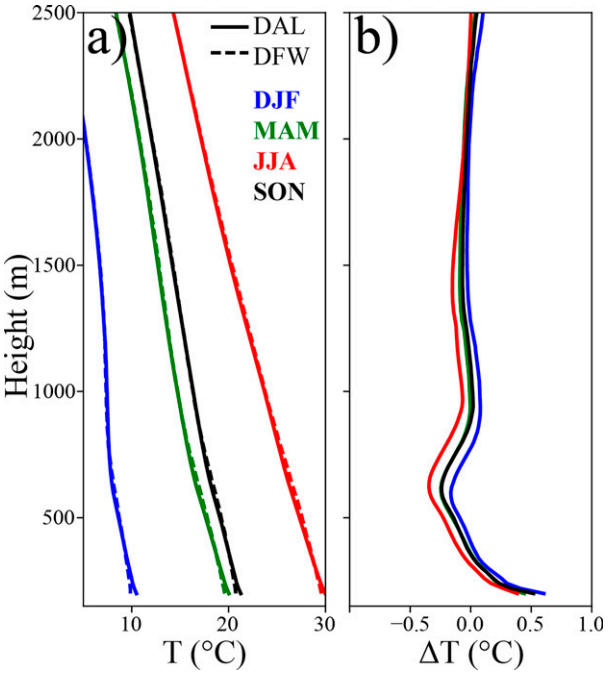

FIG. 2. (a) Average temperature (°C) profile from DAL (solid) and DFW (dashed) for DJF (blue), MAM (green), JJA (red), and SON (black). (b) Temperature (°C) difference between DAL and DFW for the four seasons.

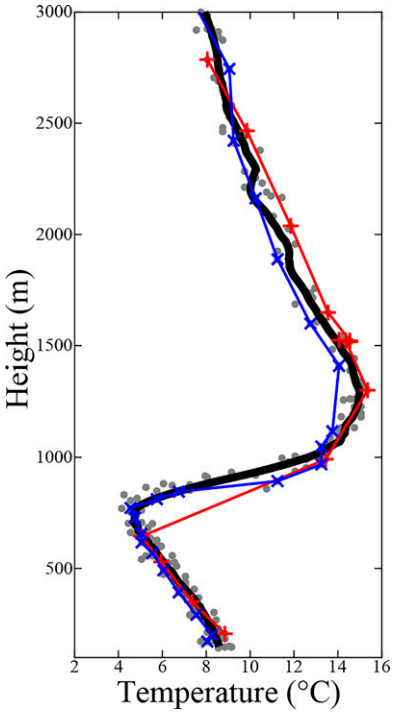

FIG. 3. All point observations of temperature (°C; gray dots) from AMDAR soundings from DAL and DFW from the 0000 UTC 22 Jan 2012 bin. Two individual profiles are highlighted in red and blue, with the symbols representing each of the respective point observations. The averaged and linearly interpolated sounding is shown by the thick black line.

Since DFW and DAL are located 18 km apart, the soundings are similar to each other. The largest differences between DFW and DAL occur when there is active weather. In fact, the temporal and vertical resolution is so good that features such as weak outflow from a nearby convective storm could be seen moving from DFW to DAL minute by minute. In the long term, averages that use all soundings tied to each airport have some subtle differences that appear between the airports (Fig. 2). DAL is slightly warmer than DFW near the surface (0.5°C) and the stability is slightly lower. Differences above the surface are less than 0.25°C. This difference can be explained by referring back to Fig. 1 and noting that the radiometric surface temperatures from MODIS are slightly higher near DAL because DAL is located in an area with a denser built environment. The subsequent analysis combines both airports, but the same analysis was also performed on the airports separately. The results using the separate airports have larger confidence intervals since the sample size decreases, but the results are not substantially different than combining data from both airports. Given that there are minor differences on average, days with active weather that cause the largest differences between airports are removed, and that the day-to-day differences are much larger than the differences between the airports, we can confidently use observations at both airports together to construct an average sounding without differentiating between the airports.

Given the inconsistent aircraft flight times and sampling levels, the data must be standardized. To take advantage of the considerable number of soundings and effectively increase the vertical resolution, multiple soundings are often used to construct a single profile (e.g., Rahn and Mitchell 2016; Zhang et al. 2019). In addition to the effective increase of vertical resolution, random measurement errors from individual soundings are damped, assuming the errors behave as white noise, and outliers more than two standard deviations were removed. Observations are binned in 30-min intervals and linearly interpolated to 20-m intervals below 3 km to create a single profile each half hour. For each of these half-hour intervals, the time of each bin relative to sunrise is found for every day. All heights are with respect to sea level.

An example is shown in Fig. 3, which shows all point observations, the linearly interpolated 20-m sounding, and two individual profiles that are also highlighted, one in blue and the other in red. The red profile demonstrates a single profile will have an erroneous BL height from the lack of vertical resolution, and the blue profile demonstrates a similar issue with the inversion layer. Only by including all observations in the time bin can we get a sharper depiction of the temperature profile and main features; this sharpness is from an effectively higher resolution. A 20-m grid spacing is selected for the average since it appears to adequately capture sharp features as seen in Fig. 3. This figure also shows more observations in the lowest part of the atmosphere and fewer near 3 km, consistent with the World Meteorological Organization (WMO) specifications for AMDAR observing intervals by flight phase (refer to Fig. 2.2 in WMO 2017).

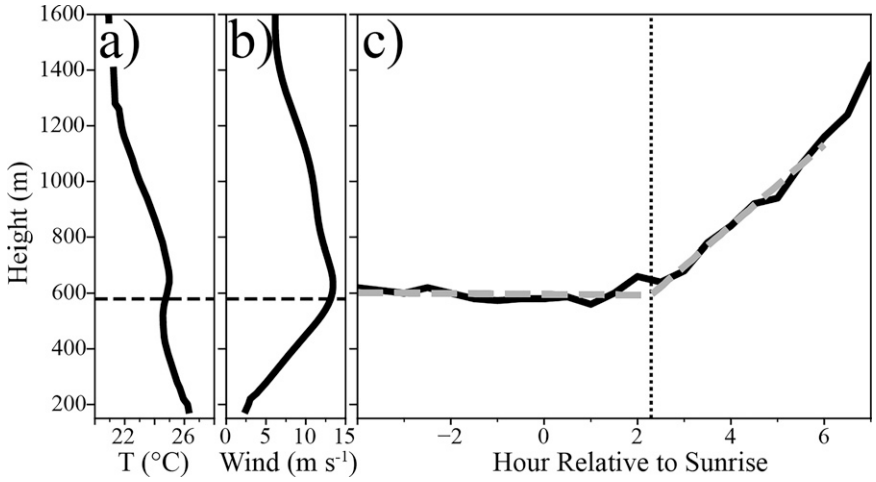

FIG. 4. Example of methods on 16 Jul 2015 showing (a) temperature (°C) profile at sunrise, (b) wind speed (m s^{-1}) profile at sunrise, and (c) time series of BL height relative to sunrise. The BL height from the Ri_{bc} method is depicted by the black line. The best piecewise linear fit lines are indicated by the gray dashed lines, with the corresponding end of the morning transition indicated by the vertical dotted line.

c. *BL identification*

The BL height can be quantified using several approaches. Each approach is constrained by available observation types and densities (Dai et al. 2014). Temperature gradients below 3 km can be used to determine inversions that often mark the top of the BL, but there may not be an inversion or a weak inversion could be missed. Because AMDAR profiles have reliable temperature and wind measurements, it is possible to estimate the BL height with the bulk Richardson number Ri_b, which is fundamentally a ratio between buoyancy and wind shear. The general concept of using the Ri_b to find the BL height has existed for some time (e.g., Hanna 1969). The exact formulation is periodically refined such as the formulation in Vogelezang and Holtslag (1996) that tends to work better with higher wind speed since it avoids overestimating the shear production in stable BLs. The Vogelezang and Holtslag (1996) formulation has been tested in Zhang et al. (2014) with a slightly revised formulation of

$$\mathrm{Ri}_b = \frac{(g/\theta_{vs})(\theta_{vz} - \theta_{vs})(z - z_s)}{(u_z - u_s)^2 + (v_z - v_s)^2 + 100u^*},$$

where z is the height of the observation; z_s is the height of the lower boundary (often the top of the surface layer, but defined as the lowest AMDAR observation here); and θ_{vz}, u_z, and v_z are the virtual potential temperature, zonal wind speed, and meridional wind speed components, respectively, at height z. The θ_{vs}, u_s, and v_s are the virtual potential temperature, zonal wind speed, and meridional wind speed components, respectively, at height z_s, and u^* is the friction velocity. Since Liu et al. (2009) found that u^* normalized by the wind speed over cities is around 0.2, we replace u^* with 0.2 multiplied by the wind speed. Virtual potential temperature is replaced by potential temperature in Eq. (1) because there are far fewer profiles that also have water vapor measurements. Using virtual potential temperature would have an impact on the values, but, given that 90% of our soundings do not have water vapor, we use potential temperature.

The height of the BL is defined when the Ri_b reaches a threshold value referred to as the critical Ri_b (Ri_{bc}; Hanna 1969). While the concept of using Ri_b and Ri_{bc} is straightforward, the calculation is sensitive to the particular way Ri_b is formulated and what Ri_{bc} is chosen (Vogelezang and Holtslag 1996; Zhang et al. 2014). Optimal thresholds for Ri_{bc} vary from 0.15 to 1.0 under different thermal stratification (Zilitinkevich and Baklanov 2002; Jericevic and Grisogono 2006; Esau and Zilitinkevich 2010), but common thresholds are 0.25 and 0.5 (Troen and Mahrt 1986; Holtslag and Boville 1993). We selected an Ri_{bc} of 0.25 to be consistent with Zhang et al. (2020).

An example of BL height determined using the Ri_b formulation above with a threshold of 0.25 is included in Figs. 4a,b. We examined sensitivity to different thresholds, but unless a very large or small value was used, there is little difference in the timing of the end of the morning transition. This is expected since changing the Ri_{bc} just shifts the BL height up or down but the slope over time is relatively unaffected. The change of slope is what is important when finding the end of the morning transition. A reasonable range of Ri_{bc} (0.15–1) only shifts the BL level slightly.

There were times with sparse data early in the data record and before sunrise that sometimes resulted in BL heights that were much different than BL heights just before or after that time. To account for this last issue, we used a 2-h moving window and removed BL heights that were 1.5 standard deviations greater than the average in that window, which removed BL heights in 4% of the half-hourly bins.

d. Case selection

Since the focus is on the duration of the morning transition, days with active weather, such as frontal passages or convection that can dominate the forcing of the BL, need to be avoided. Days with any precipitation recorded at the surface stations are removed. Even if there is no precipitation, substantial cloud cover can accompany these transient synoptic events. Additionally, clouds in the BL overnight will help maintain a well-mixed layer down to the surface from top-down turbulent mixing driven by longwave cooling at cloud top and downward longwave radiation from the cloud layer. So, cloud observations from the Automated Surface Observing System (ASOS) are used to find and then exclude days where the average cloud cover 5 h before and 5 h after sunrise is above 4 oktas. It is recognized that clouds play a substantial role, but removing this factor using surface observations helps to constrain the analysis. The last criterion for case selection deals with days that were clear but postfrontal, where the structure of the lower atmosphere was still dominated by transient features. So, clear days with northerly wind are also excluded.

e. Identifying the end of the morning transition

After finding the BL height for each 0.5-h interval, the next step is to identify when the morning transition ends. The morning transition period can be identified using changes in near-surface wind, near-surface heat flux sign, or the moment when convection reaches 200 m (e.g., Angevine et al. 2001; Lapworth 2006). Changes in near-surface wind are a crude way to determine the morning transition, and it is also difficult to use wind near the surface in an urban environment given that the surface heterogeneity casts doubt on the representativeness of the point measurement. Using a negative to positive change of sensible heat flux is incompatible for this study because there is no long-term measurement near the airports. Using a threshold of 200 m is not applicable since the BL height may already be greater than 200 m at night. Also, 200 m was used arbitrarily because it was the height of the tower used in the study by Angevine et al. (2001).

The most applicable method for finding the end of the morning transition is to identify when the onset of the rapid mixed-layer growth occurs similar to Halios and Barlow (2018). A typical example of the BL time series derived from AMDAR is show in Fig. 4c. All time series are standardized to local sunrise. There is a clear shift in the time series from a relatively constant BL height to a rapid growth phase. Many methods may be used to identify prominent shifts in time series, which are referred to as breakpoint or changepoint methods (Reeves et al. 2007; Lund et al. 2007). Since we are interested in finding the initial change from the relatively constant BL height before the end of the morning transition and the rapid change of BL height during the initial growth phase, we select a window that starts 4 h before sunrise and ends 6 h after sunrise. Within this 10-h window, we use a simple linear regression to fit the data before and after each possible break point. If the window is extended later than this, then there are issues with using a linear regression since the BL growth rate slows greatly as the mature phase of the BL begins. The most likely break point is selected by finding the minimum mean square error among all of the pairs of fitted lines.

Although the method works well in most situations, it is susceptible to spurious BL heights. The major outliers of the BL heights are removed as discussed in the previous section, but days with fewer observations, especially early in the record, tend to have larger variance that can impact the detection of the end of the morning transition. Also, early in the record there can be too few observations around sunrise to be useful, so these are excluded. An underlying assumption of this breakpoint method is the linearity of the BL height during the several hours before and after the end of the morning transition. The BL height time series on some days does not exhibit linear behavior, but nonetheless the linear regression still picks up the time when there is the most rapid change of slope. Finally, even though many days with active weather that dominate the diurnal signal are filtered out, there are still days that do not exhibit the ideal features of a relatively constant BL height around sunrise that transitions into a rapid growth phase later in the day. Some days have a BL height that remains essentially unchanged over the entire window. To handle ambiguous breakpoints of the daily time series, if the slope of the rapid growth phase is less than 30 m h^{-1}, if the slope is greater before the end of the morning transition than after the end of the morning transition, or if the breakpoint occurs before sunrise, then the time of the end of the morning transition is considered ambiguous and excluded. Of the 2006 days after the initial filtering of precipitation, cloud, and northerly wind, there are 1678 days (84%) that have unambiguous morning transition periods and that were used in this study. Since 23% of the total days during the 20-yr period were used in this study, this reduces the number of AMDAR profiles used. It also points to the utility of having AMDAR observations available every day so that a sufficient volume of observations is available for longer-term studies that contain appropriate filtering techniques.

3. Results

a. Baseline characteristics

Results are separated by season as December–February (DJF), March–May (MAM), June–August (JJA), and September–November (SON), and exclude days that have northerly winds, are cloudy, or have precipitation. The seasonal distribution of BL heights relative to sunrise is provided in Fig. 5. As expected, deeper BLs tend to occur during the summer months and are lowest during winter. For times earlier than about two hours after sunrise, the distribution of the BL heights is generally steady and have a fairly constant median with a tail skewed slightly toward higher heights. These boxplots also demonstrate that deep BLs in the morning are rare, so the selection criteria are effective at removing mornings with deep BLs driven by transient weather or cloudy BLs, so we are able to isolate and examine the morning transition. Later in the day the mean and median increase quickly and the

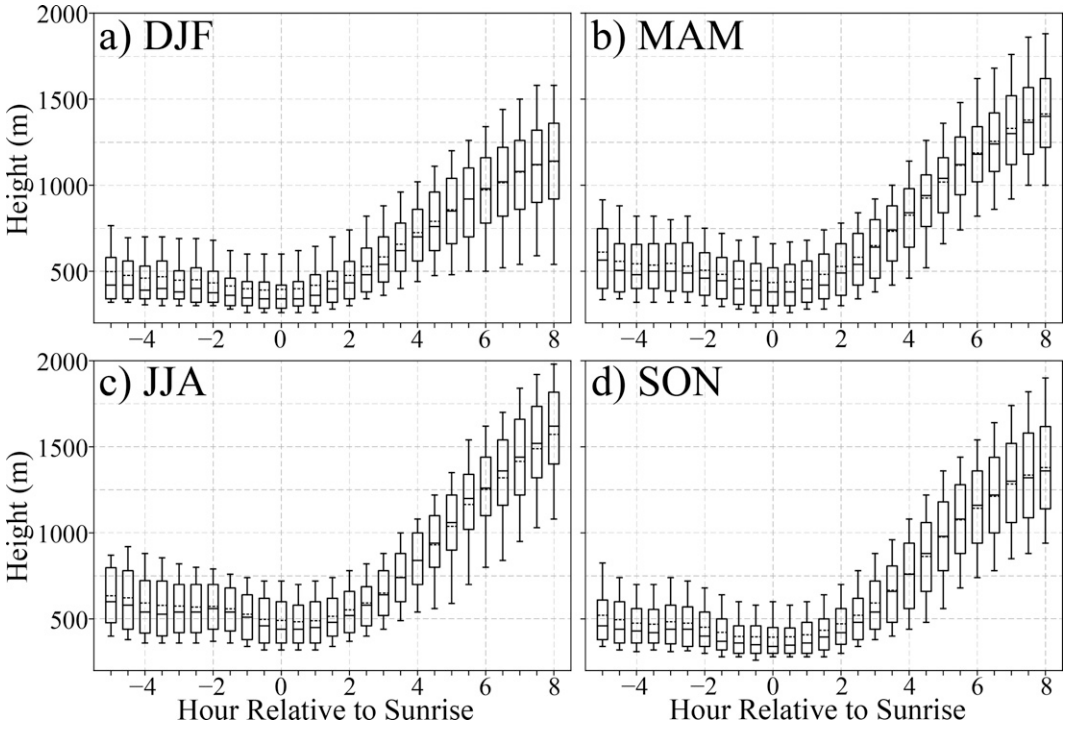

FIG. 5. Boxplots of BL height for selected cases showing the interquartile range (box) with whiskers extending to the 10th and 90th percentiles and the median (solid) and mean (dashed) shown inside the box for (a) DJF, (b) MAM, (c) JJA, and (d) SON.

distribution widens. Days without a clear morning transition period tend to happen when the BL undergoes little change throughout the day.

Although the Ri_b method provides an estimate of the BL height, there is no information on the structure of the atmosphere within the BL. In particular, it is the stability in the BL that is most relevant since it is not only associated with trapping pollution, but it is what must be overcome to begin the rapid growth phase of the daytime BL. To summarize the stability within the BL, the lapse rate of the layer extending from the surface to the top of the BL is calculated for each sounding by taking a linear regression of the temperature profile in this layer. Lapse rates are binned into four categories to aid in the interpretation. Lapse rates $< -2°C\ km^{-1}$ represent profiles with a temperature inversion. Lapse rates between $-2°$ and $4°C\ km^{-1}$ represent profiles that are closest to isothermal, which is the rarest profile. Lapse rates between $4°$ and $8°C\ km^{-1}$ are profiles that are approaching a well-mixed layer. Lapse rates $> 8°C\ km^{-1}$ are sufficiently close to the dry adiabatic lapse rate that the profile can be considered to be a well-mixed layer. The distribution of lapse rates for each hour relative to sunrise over each season is depicted in Fig. 6.

Because this study was limited to days with few to no clouds, inversions are common before sunrise, as highlighted in Fig. 5. There is a notable exception for JJA when temperature inversions are much less common. From 0 to 2 h before sunrise, temperature inversions occur about 20% of the time in JJA, but during other seasons inversions occur 70%–90% of the time. Lapse rates $< -2°C\ km^{-1}$ before sunrise occur over a much larger fraction of the time in the other seasons, approaching 90% of the time in DJF and 80% of the time in MAM and SON, and the inversion persists longer after the sun rises than during JJA. In all of the seasons, the time series of lapse rates indicate a rapid erosion of the inversion that is evident in the steep slope around two hours after sunrise. The rapid erosion can also be inferred by the fraction of time where the lapse rate is approaching well mixed ($4°$–$8°C\ km^{-1}$) since this category makes up about ~70% of the profiles 2–3 h before sunrise.

While the distributions of lapse rates seen in Fig. 6 are not particularly surprising, the distributions illustrated here both exhibit the ability of how much detailed information that AMDAR observations can provide over the city and also will aid in explaining the features of the morning transition shown later. In particular, during summer over Dallas–Fort Worth when skies are clear, there is only an inversion above the city about 30% of the time before sunrise whereas 60% of the time the lapse rate was at least $4°C\ km^{-1}$. A smaller fraction of the mornings exhibits a strong inversion near the surface when compared with other times of year, which is related to shorter nights and higher water vapor during summer.

b. *Influence of wind*

To begin to differentiate the behavior of the lower atmosphere caused by southerly wind speed, the BL height at sunrise for each season is plotted as a function of maximum wind

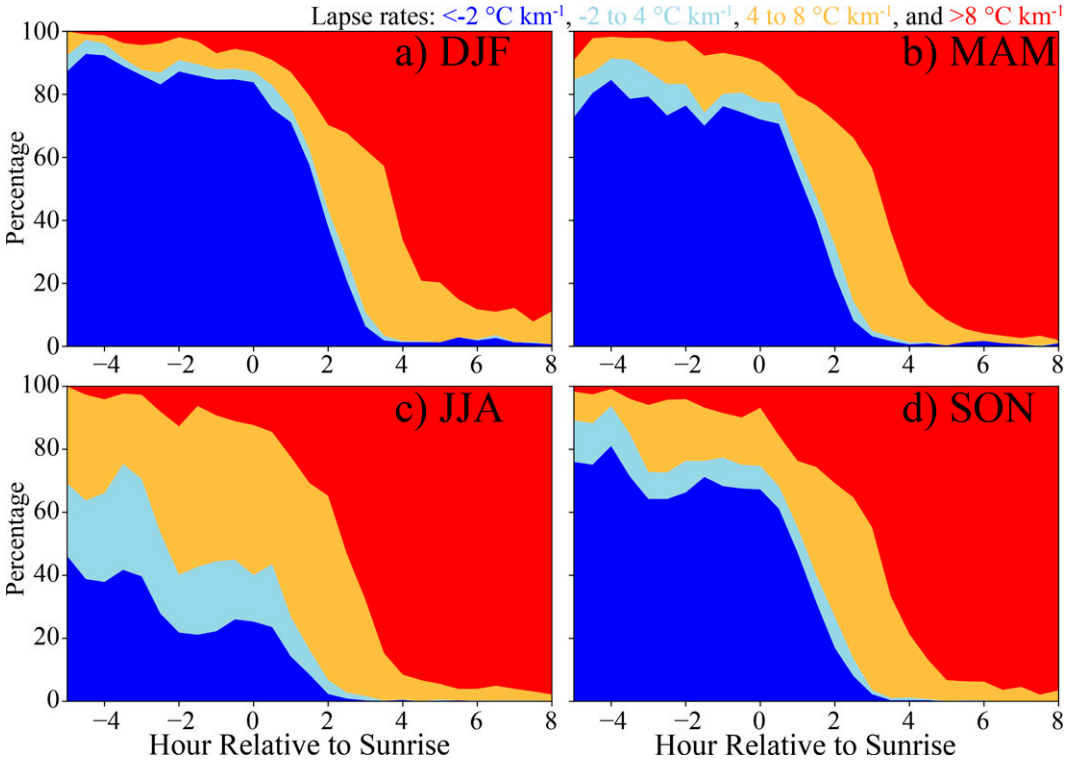

FIG. 6. Percentage of time that each lapse rate (°C km^{-1}) category was present relative to sunrise for (a) DJF, (b) MAM, (c) JJA, and (d) SON.

speed below 1400 m from profiles averaged 1 h before and after sunrise in Fig. 7. Climatologically, low-level winds caused by the LLJ are not higher than 1400 m (e.g., Song et al. 2005), so this value is chosen as the upper limit to search for a local maximum of wind speed. For wind speeds less than about 5 m s^{-1}, there is little difference of BL height between the seasons with the exception of JJA, which is slightly higher and consistent with a less stable lower atmosphere. Following the ideas of threshold winds driving a deeper mixed layer (e.g., Sun et al. 2012; Bonin et al. 2015), if there is an obvious abrupt change of BL depth as wind speed increases, then that would signify a threshold. In these seasonal averages, there are no sharp discontinuities, but there are some differences between seasons with regard to the minimum wind speed where the BL height begins to noticeably increase with an increasing wind speed. This occurs after 5 m s^{-1} for JJA, SON, and MAM, but for DJF this occurs after 10 m s^{-1}. Given the relationship between wind and BL height from this figure, wind speeds categories used for subsequent figures use bins every 5 m s^{-1}.

After filtering out days with precipitation, clouds, and northerly wind, we take two approaches to quantify the relationship between the maximum wind speed below 1400 m at sunrise and the end of the morning transition: 1) use the average of the daily end times of the morning transitions in each wind category, and 2) find the average BL height time series for each wind category and then find the end of the morning transition from that average.

1) DAILY TRANSITIONS

The first approach is to use the filtered days and then find the end of the morning transition for each day using the breakpoint method. The distributions of morning transition durations for each wind category and season are represented by normalized kernel density plots in Fig. 8. Histograms with

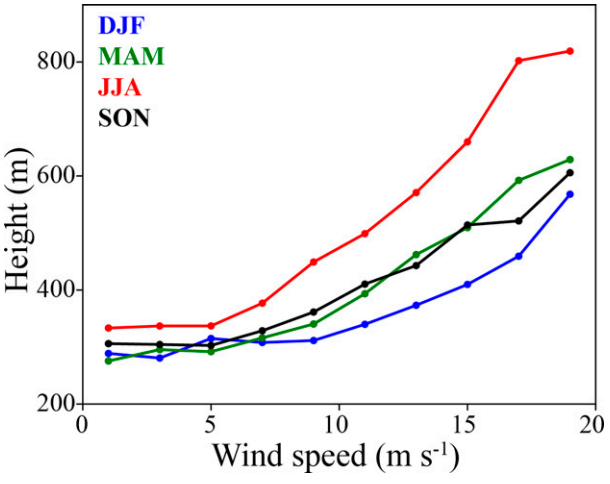

FIG. 7. Average BL height at a 2-h window around sunrise (m) for each season, binned by maximum wind speed below 1400 m at sunrise every 2 m s^{-1}.

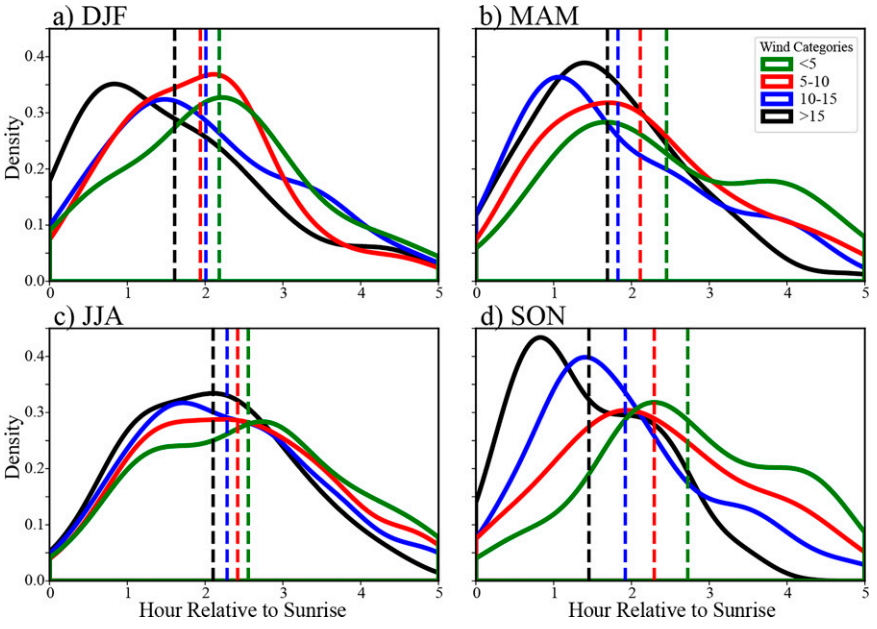

FIG. 8. Normalized distribution of the morning transition duration relative to sunrise in each wind category [as indicated in the legend in (b)] for (a) DJF, (b) MAM, (c) JJA, and (d) SON. The mean of each distribution is indicated by the dashed lines.

four bars for each bin are difficult to interpret, so we are using kernel density plots since they are much cleaner and easier to interpret. The mean of each distribution, the 95% confidence interval of each mean, the number of samples in each distribution, and percent contribution from each season are provided in Table 1. It is clear to see that summer (JJA) has the greatest number of total days used, followed by autumn (SON) and then spring (MAM). After removing northerly wind, clouds, and precipitation, there are 26% of the total days remaining. Most distributions have a single prominent peak, are broad since they extend over much of the window, are skewed to the right, and reveal that the distribution and its mean shifts toward shorter morning transition durations as the wind speed increases. This shift is evident in each season with SON showing the greatest difference between the distribution shapes and the associated average morning transition duration, which range from 2.72 h after sunrise for wind speeds <5 m s^{-1} to 1.45 h for wind speeds >15 m s^{-1}. An exception to the relationship between the mean wind speed and morning transition duration occurs for the middle two wind categories during DJF; however, there is no significant difference between the means. Several other neighboring categories are not significantly different from each other, but most categories that are at least one step apart are significantly different.

During summer (JJA), the distribution of daily morning transition durations and their means reveal the smallest differences between the wind categories and the distributions exhibit less skewness. The morning transition duration when winds are >15 m s^{-1} is at least half an hour longer on average than the other seasons. This is in contrast to SON when the frequency of having a morning transition duration of an hour or less is much greater.

2) SEASONALLY AVERAGED TRANSITION BY SPEED GROUPS

The second approach to relate morning transition duration to the wind speed takes all of the BL height time series relative to sunrise for each season and wind category, creates an average time series for each category, and then the uses the breakpoint method to find the end of the morning transition from that average time series. The results are shown in Fig. 9, and the associated mean, sample sizes and percent contribution from each season are provided in Table 2. Note that there

TABLE 1. Corresponding to Fig. 8, individual morning transition duration (h) with 95% confidence intervals and with sample sizes in parentheses. Total days (%) per season and in total with respect to the unfiltered data are also given.

Wind category	DJF	MAM	JJA	SON	All
<5 m s^{-1}	2.18 ± 0.37 (29)	2.45 ± 0.35 (39)	2.56 ± 0.23 (78)	2.72 ± 0.20 (97)	2.56 ± 0.13 (243)
5–10 m s^{-1}	1.94 ± 0.18 (90)	2.11 ± 0.22 (85)	2.42 ± 0.13 (235)	2.30 ± 0.14 (200)	2.27 ± 0.08 (610)
10–15 m s^{-1}	2.01 ± 0.23 (75)	1.83 ± 0.22 (81)	2.28 ± 0.13 (231)	1.92 ± 0.14 (164)	2.07 ± 0.08 (551)
>15 m s^{-1}	1.61 ± 0.23 (69)	1.69 ± 0.19 (74)	2.11 ± 0.22 (63)	1.45 ± 0.18 (68)	1.71 ± 0.10 (274)
Total days (%)	16%	17%	37%	32%	26%

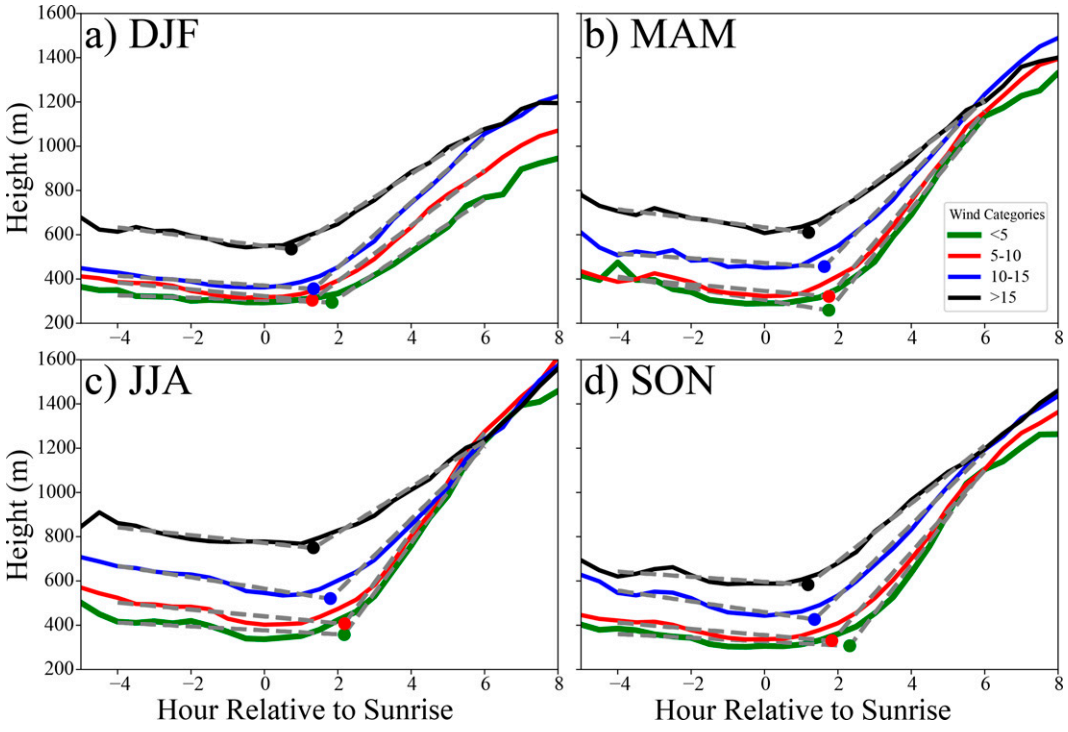

FIG. 9. Time series of the average BL height in each wind category [as indicated in the legend of (b)] for (a) DJF, (b) MAM, (c) JJA, and (d) SON relative to sunrise. The best piecewise linear fit lines are indicated by the gray dashed lines, with the corresponding end of the morning transition indicated by a circle.

are more samples, in total and with respect to the total number of days, using this method than using the daily morning transition duration since days when the morning transition was ambiguous were still able to be included in the averages. The figure is essentially unchanged if the subset from the previous method is used. However, there are still relatively more days during summer (JJA) and autumn (SON), and the total number of days for all the seasons increased from 26% to 31%.

Averaging BL heights over each wind category results in less-sharp transitions between the relatively steady BL height before the end of the morning transition and the rapid growth phase afterward that is sharper in the individual daily time series. This makes the assumption less appropriate for some categories that two piecewise linear regressions are the best representation for the averaged time series, but the estimate of the end of the morning transition from the breakpoint is still reasonable and generally consistent with the first method.

All morning transition durations are shorter using this approach rather than taking the average of the individual morning transition durations. The average difference is about half an hour earlier. However, the tendency of the end of the morning transition to occur earlier when wind speeds are greater still holds with the same exception as seen previously that occurs with the two middle wind categories during DJF. The difference between the first two wind categories during MAM and JJA are also small using this method. Unlike the previous method, there is a larger difference in the end of the morning transition between the lowest and highest wind categories during JJA.

From Fig. 9, it is clear to see several other features occurring with the lower atmosphere that are expected. First, the average BL heights are higher during the warmer seasons. Second, the BL heights are higher when the wind speed is greater. The difference of BL height between the lowest two wind categories is small. During DJF, only the highest wind

TABLE 2. Corresponding to Fig. 9, group-averaged morning transition duration (h), with sample size in parentheses. Total days (%) per season and in total with respect to the unfiltered data are also given.

Wind category	DJF	MAM	JJA	SON	All
<5 m s^{-1}	1.84 (36)	1.75 (48)	2.18 (99)	2.32 (113)	2.19 (296)
5–10 m s^{-1}	1.30 (113)	1.76 (95)	2.19 (284)	1.83 (235)	1.81 (727)
10–15 m s^{-1}	1.34 (90)	1.63 (93)	1.80 (281)	1.36 (178)	1.69 (642)
>15 m s^{-1}	0.73 (100)	1.20 (90)	1.33 (75)	1.18 (76)	1.14 (341)
Total days (%)	21%	20%	45%	37%	31%

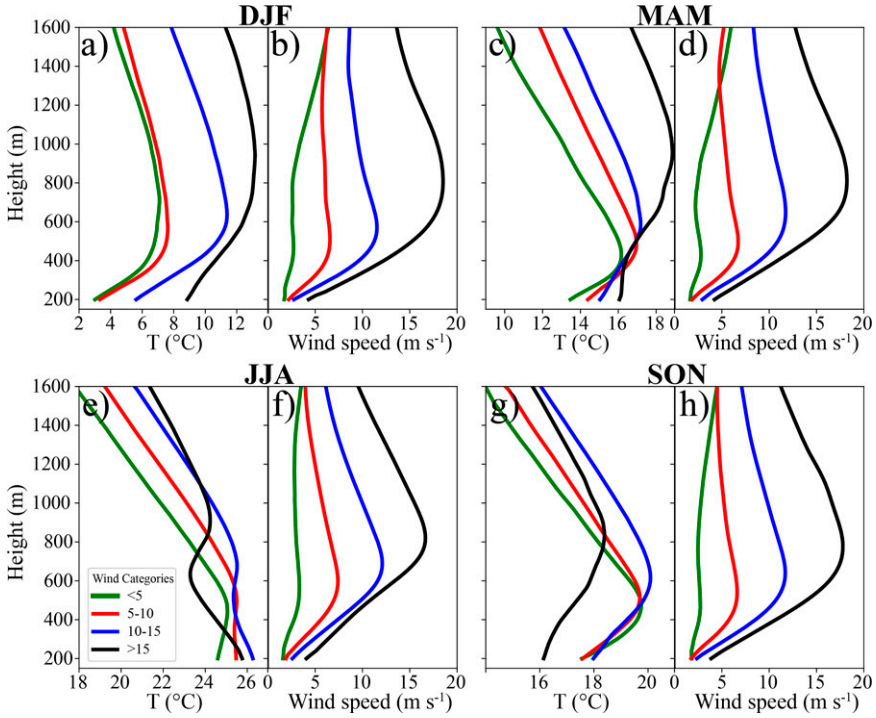

FIG. 10. Average profiles of temperature (°C) and wind speed (m s^{-1}) at sunrise using the criteria given in section 2d binned by wind speed category [indicated in the legend of (e)] for DJF, MAM, JJA, and SON. Note that the temperature ranges are not the same for all seasons.

category has a BL height that is clearly set apart from the rest, which is consistent with Fig. 7 that showed that the BL height changed the least with wind speed during DJF. For seasons other than DJF, the BL height in both the 10–15 and also >15 m s^{-1} categories are substantially higher than the lowest two wind categories. Third, the growth rates of the BL height after the end of the morning transition are slower for higher wind speed with all BL heights becoming similar about 6 h after sunrise.

3) AVERAGE PROFILES

The average profiles at sunrise of temperature (°C) and wind speed (m s^{-1}) for each season and wind category using the criteria given in section 2d are depicted in Fig. 10. A distinct local wind maximum is evident in all wind speed profiles except the weakest wind category. The height of the local maximum increases as the maximum wind speed increases, which is consistent with other climatologies of the LLJ (e.g., Song et al. 2005). A surface temperature inversion is evident in almost all of these average profiles at sunrise, consistent with the lapse rates in Fig. 6. The surface temperature inversion is the most pronounced when the wind is weakest and during DJF. The depth of the surface inversion increases as the maximum wind speed below 1400 m strengthens. A surface inversion is not present in JJA when the wind is above 5 m s^{-1}. The atmosphere is isothermal when the wind is 5–10 m s^{-1} and is nearly well-mixed for higher wind speeds. When the wind is above 15 m s^{-1}, the well-mixed layer is the deepest and capped by a strong elevated inversion. The only time outside of JJA that does not have a strong temperature inversion is during MAM under the strongest wind conditions.

To understand the evolution of the temperature profiles, time series of the lapse rate are provided for JJA and MAM (Fig. 11), excluding days described in section 2d. The lapse rates are found from the average profiles at each half-hourly interval as in Fig. 10, and the lapse rate is found by taking the temperature difference above and below each level and dividing by 40 m. The time series for SON and DJF are similar to MAM, but slightly more intense so only MAM is shown for brevity. Similar to the profiles at sunrise (Fig. 10), MAM displays a strong inversion in the BL (as shown in the Fig. 11) during the early morning for the first three wind categories. When the winds are > 15 m s^{-1}, the lapse rates near the surface are close to an isothermal profile on average with a stable layer above coincident with the average BL height. In contrast, JJA exhibits a less stable BL with a nearly isothermal BL on average for the first two wind categories and becoming more well-mixed with higher wind speeds. A stable layer also appears at the top of the BL for several hours around sunrise, which increases in strength at high wind speeds.

Lapse rates above the average BL tend to be steeper for the lightest winds and during summer, possibly reflecting a residual layer from the day before. For the lightest winds, the rate of BL growth after the end of the morning transition is

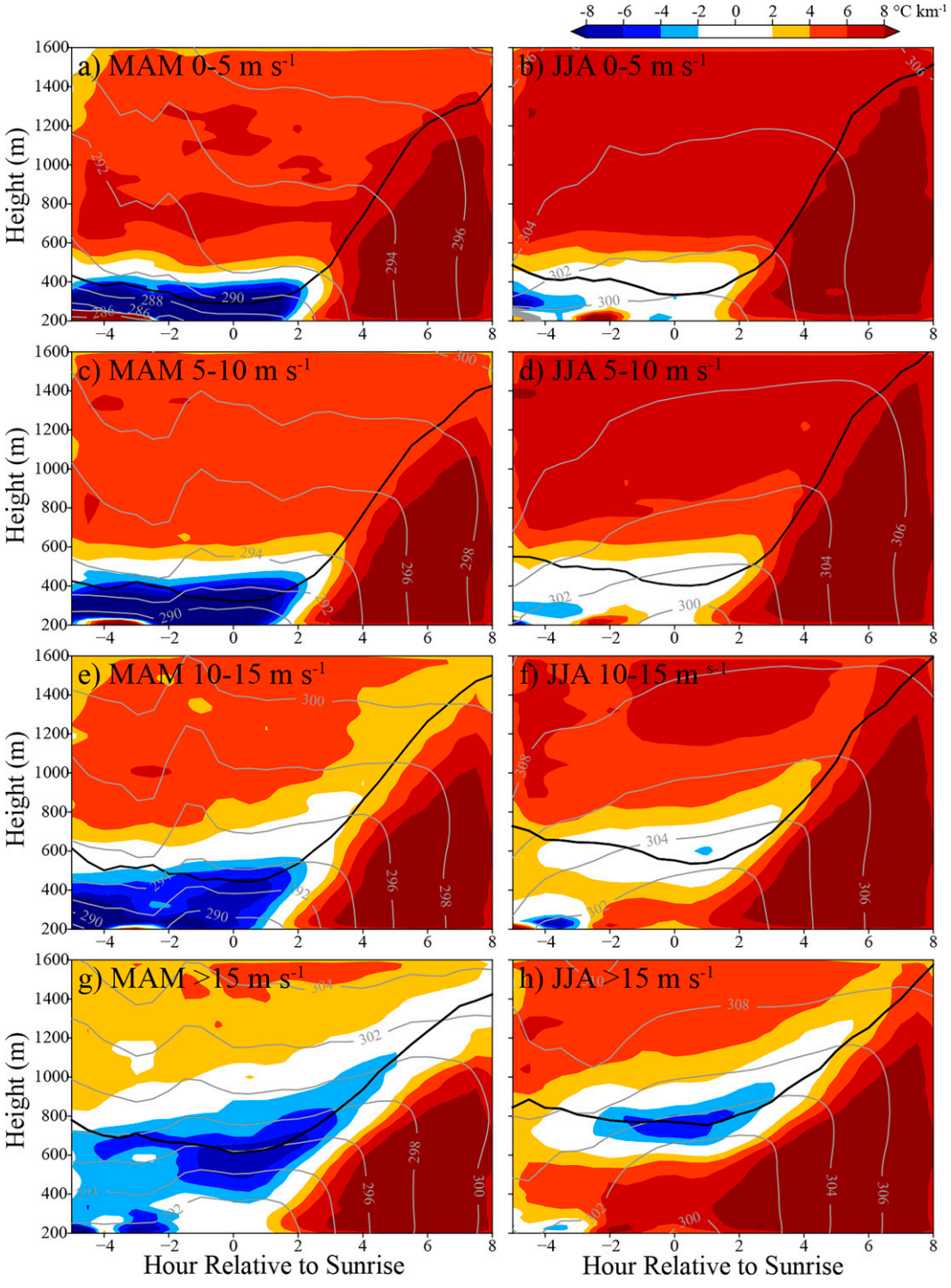

FIG. 11. Evolution of the lapse-rate profile (°C km^{-1}) relative to sunrise for (left) MAM and (right) JJA for each wind category, with the mean BL height profile (black contour) and potential temperature (K; gray contours).

the most rapid since it is likely that as soon as the residual layer is reached, mixing is much easier given the reduced stability in the residual layer. This is in contrast to days with the strongest winds where an inversion that exists before sunrise persists later into the day. The BL begins much higher and less stable with relatively slow growth rates given that there is no rapid growth associated with reaching the residual layer that occurs when there are lighter winds.

4. Summary and conclusions

Understanding the lower atmosphere over urban areas is an important issue, but it is often a difficult task because of the complexity of processes taking place over highly heterogeneous surfaces of the built environment. Part of the difficulty comes from a simple lack of measurements. Here, we demonstrate the capability of compiling and processing the 1.5 million high-time-frequency aircraft-based AMDAR soundings over the Dallas–Fort Worth region to examine the morning transition. The ample number of observations over the last two decades provides many details of the lower atmosphere, including evolution of the BL lapse rates around sunrise that are difficult to assess with any other operational observing system. AMDAR reports capture details of the evolution of the lower atmosphere with at least half-hourly intervals over this urban area. The growth of the AMDAR program since 2000 provides an immense quantity of measurements. The quality and frequency of AMDAR measurements are excellent. Observations in the BL are tied to major airports, and so their spatial resolution is somewhat limited. Airports are not necessarily located at the center of an UHI, and therefore not all locations represent urban BLs.

The Dallas–Fort Worth region is an ideal location to examine the urban BL since there is a high volume of air traffic near the UHI core and the area is not influenced by any major topographic or coastal features. Other than transient synoptic systems, the nocturnal LLJ is often a major factor associated with the day-to-day variability of the weather. In particular, the UHI is greatly impacted by the categorical strength of the LLJ such that weak LLJs have a more pronounced UHI while strong LLJs have a weaker UHI (Hu et al. 2013). In this study, we examine duration of the morning transition, stability, and other features by also using categories of southerly wind speed. Given that DAL and DFW are only 18 km apart, the profiles are nearly identical, but DAL tends to be slightly warmer and less stable than DFW, probably because it is located near a denser part of the city. So, observations from both airports are used to find a single average profile each half hour.

The key feature that motivated this work, which can now be quantified given the long record of frequent and high quality observations from AMDAR, is the morning transition from a shallow BL at sunrise to the rapid growth phase. Observations were binned every half hour and linearly interpolated to 20-m intervals to create one sounding every half hour. The time relative to sunrise is found for each bin. To focus on the morning transition, days that were cloudy, had precipitation, winds from the north, or an ambiguous morning transition duration were removed leaving 1678 days (26%) over the 2001–20 period. Under these constraints, time series of BL height followed the expected morning cycle of low and relatively steady BL heights near the surface before sunrise followed by rapid lifting of the BL several hours after sunrise.

At and prior to sunrise, there was almost always a temperature inversion immediately above the surface over the city with the notable exception of JJA when a surface temperature inversion occurred less than 30% of the time. An elevated inversion at sunrise was the strongest during high wind in JJA, and the strong elevated inversion is likely to persist longer than weaker inversions.

The duration of the morning transition decreases with increasing wind speed, as shown by both taking the means of the daily morning transitions (Fig. 8) and also by averaging the time series of BL heights and then finding the duration of the morning transition of that averaged time series (Fig. 9). The differences of morning transition durations between the lightest and strongest wind categories are on the order of an hour with the greatest difference of 1.27 h for the individual averages occurring in SON. For some of the consecutive wind categories, there is overlap in the 95% confidence intervals and the differences are not significant (Table 1). For almost all of the wind categories at least one step apart, the differences are significantly different. The distribution of morning transition duration as a function of wind speed is the most similar in JJA and the least similar in SON.

A reason for the similar distribution of morning transition durations during JJA can be linked to some mitigating factors that are more prominent in JJA. The average BL height at sunrise as a function of wind speed (Fig. 7) indicated a slightly higher BL at low wind speeds during JJA that deepens with wind speed at a rate much greater than other seasons. Furthermore, the averages of the daily time series for each wind category and season (Fig. 9) indicate that the BL at sunrise is not only generally higher during JJA, but it also deepens more per wind category than any other season. Given a deeper BL at sunrise to begin with, the same amount of warming from insolation would be distributed over a larger depth given the initially deep BL, so the average warming of the layer would be much less than that of a shallow layer. The amount of warming scales linearly such that the amount of heating is halved for a BL that is twice as deep and the corresponding growth rate would also be half as much. Given that JJA has the largest increase of BL depth with wind speed, the much deeper initial BL at high wind speeds would slow growth rates, partially counteracting the increase of growth rates associated with stronger wind speeds leading to the smallest difference of morning transition durations in JJA.

The relationships between the southerly low-level wind and structure of the lower atmosphere including BL height, lapse rate, and morning transition duration when excluding clouds and precipitation are clearly evident using information from the high-quality and frequent AMDAR observations over Dallas–Fort Worth. By establishing the ability of AMDAR to be used to assess such detailed features as the near surface inversion and shifts in the morning transition over the city, these can be used with other datasets such as air pollution or can provide the basis for any model comparison. Furthermore, the potential benefits of developing these relationships are particularly relevant to forecasters, particularly in the National Weather Service, that have real-time access to AMDAR observations. While it is difficult to make sweeping generalizations with just the observations alone, we demonstrate that these measurements can be essential in establishing the baseline response of the lower atmosphere over an urbanized area. Not only should all of the factors responsible for

eroding a surface inversion be considered such as background synoptic conditions, sky conditions, low-level wind, initial low-level stability, and so on, but also it is important to consider differences between model forecast soundings over a city and current AMDAR observations that could point to deficiencies in the model solution. We emphasize that simulations can still struggle over urban areas (e.g., Wang and Hu 2021) and that this work shows the utility of AMDAR's high spatial and temporal resolution, which will be valuable when using in conjunction with numerical simulations.

There is still much future work to be done given the complexity of a city's built environment and how it relates to land–atmosphere processes. AMDAR observations will likely be an important component to expanding our understanding of the urban BL because, as demonstrated here, the measurements provide high-vertical-resolution and high-temporal-resolution measurements of temperature and wind that can capture many salient features. With water vapor measurements becoming more common, this will only increase the utility of AMDAR measurements to examine processes in more detail. The understanding of the baseline meteorology obtained from this study forms the framework for additional studies. In conjunction with numerical simulations, satellite observations, flux towers, and other observations, urban BL dynamics can be explored and questions such as the relative contributions of the local built environment and background meteorology can be investigated. Given the large biases in numerical simulations over cities, these biases can be better understood when comparing with AMDAR data and can help direct us to sources of errors and help improve models. Processes such as the relative contribution between mechanically or thermally driven turbulence can be investigated with AMDAR and additional observations in the city. In short, we encourage a broader use of AMDAR data to investigate the complex urban BL.

Acknowledgments. We thank the reviewers for their constructive comments.

Data availability statement. Observations from surface stations and aircraft that are older than 48 h are publicly available on the Meteorological Assimilation Data Ingest System (MADIS; https://madis-data.ncep.noaa.gov). Data are available for real-time use by federal agencies, including NOAA.

REFERENCES

Angevine, W. M., H. K. Baltink, and F. C. Bosveld, 2001: Observations of the morning transition of the convective boundary layer. *Bound.-Layer Meteor.*, **101**, 209–227, https://doi.org/10.1023/A:1019264716195.

Arnfield, A. J., 2003: Two decades of urban climate research: A review of turbulence, exchanges of energy and water, and the urban heat island. *Int. J. Climatol.*, **23**, 1–26, https://doi.org/10.1002/joc.859.

Azevedo, J. A., L. Chapman, and C. L. Muller, 2016: Quantifying the daytime and night-time urban heat island in Birmingham, UK: A comparison of satellite derived land surface temperature and high resolution air temperature observations. *Remote Sens.*, **8**, 153, https://doi.org/10.3390/rs8020153.

Ballish, B. A., and V. K. Kumar, 2008: Systematic differences in aircraft and radiosonde temperatures. *Bull. Amer. Meteor. Soc.*, **89**, 1689–1708, https://doi.org/10.1175/2008BAMS2332.1.

Banta, R. M., Y. L. Pichugina, and W. A. Brewer, 2006: Turbulent velocity-variance profiles in the stable boundary layer generated by a nocturnal low-level jet. *J. Atmos. Sci.*, **63**, 2700–2719, https://doi.org/10.1175/JAS3776.1.

——, ——, N. D. Kelley, R. M. Hardesty, and W. A. Brewer, 2013: Wind energy meteorology: Insight into wind properties in the turbine-rotor layer of the atmosphere from high-resolution Doppler lidar. *Bull. Amer. Meteor. Soc.*, **94**, 883–902, https://doi.org/10.1175/BAMS-D-11-00057.1.

Basara, J. B., P. K. Hall, A. J. Schroeder, B. G. Illston, and K. L. Nemunaitis, 2008: Diurnal cycle of the Oklahoma City urban heat island. *J. Geophys. Res.*, **113**, D20109, https://doi.org/10.1029/2008JD010311.

Blackadar, A. K., 1957: Boundary layer wind maxima and their significance for the growth of nocturnal inversions. *Bull. Amer. Meteor. Soc.*, **38**, 283–290, https://doi.org/10.1175/1520-0477-38.5.283.

Bonin, T. A., W. G. Blumberg, P. M. Klein, and P. B. Chilson, 2015: Thermodynamic and turbulence characteristics of the southern Great Plains nocturnal boundary layer under differing turbulent regimes. *Bound.-Layer Meteor.*, **157**, 401–420, https://doi.org/10.1007/s10546-015-0072-2.

Brunsell, N. A., D. A. Rahn, and D. B. Mechem, 2021: Impact of a nocturnal low-level jet on surface-layer turbulent characteristics. *J. Geophys. Res. Atmos.*, **126**, e2020JD034083, https://doi.org/10.1029/2020JD034083.

Chen, F., and Coauthors, 2011: The integrated WRF/urban modelling system: Development, evaluation, and applications to urban environmental problems. *Int. J. Climatol.*, **31**, 273–288, https://doi.org/10.1002/joc.2158.

Dai, C., Q. Wang, J. A. Kalogiros, D. H. Lenschow, Z. Gao, and M. Zhou, 2014: Determining boundary-layer height from aircraft measurements. *Bound.-Layer Meteor.*, **152**, 277–302, https://doi.org/10.1007/s10546-014-9929-z.

Deppe, A. J., W. A. Gallus Jr., and E. S. Takle, 2013: A WRF ensemble for improved wind speed forecasts at turbine height. *Wea. Forecasting*, **28**, 212–228, https://doi.org/10.1175/WAF-D-11-00112.1.

Duarte, H. F., M. Y. Leclerc, and G. Zhang, 2012: Assessing the shear-sheltering theory applied to low-level jets in the nocturnal stable boundary layer. *Theor. Appl. Climatol.*, **110**, 359–371, https://doi.org/10.1007/s00704-012-0621-2.

Esau, I., and S. Zilitinkevich, 2010: On the role of the planetary boundary layer depth in the climate system. *Adv. Sci. Res.*, **4**, 63–69, https://doi.org/10.5194/asr-4-63-2010.

Gebauer, J. G., and A. Shapiro, 2019: Clarifying the baroclinic contribution to the great plains low-level jet frequency maximum. *Mon. Wea. Rev.*, **147**, 3481–3493, https://doi.org/10.1175/MWR-D-19-0024.1.

Gupta, S. K., and S. P. Elumalai, 2019: Dependence of urban air pollutants on morning/evening peak hours and seasons. *Arch. Environ. Contam. Toxicol.*, **76**, 572–590, https://doi.org/10.1007/s00244-019-00616-x.

Ha, K.-J., and L. Mahrt, 2001: Simple inclusion of z-less turbulence within and above the modeled nocturnal boundary layer. *Mon. Wea. Rev.*, **129**, 2136–2143, https://doi.org/10.1175/1520-0493(2001)129<2136:SIOZLT>2.0.CO;2.

Hafner, J., and S. Q. Kidder, 1999: Urban heat island modeling in conjunction with satellite-derived surface/soil parameters. *J. Appl. Meteor.*, **38**, 448–465, https://doi.org/10.1175/1520-0450(1999)038<0448:UHIMIC>2.0.CO;2.

Halios, C. H., and J. F. Barlow, 2018: Observations of the morning development of the urban boundary layer over London, UK, taken during the actual project. *Bound.-Layer Meteor.*, **166**, 395–422, https://doi.org/10.1007/s10546-017-0300-z.

Hanna, S. R., 1969: The thickness of the planetary boundary layer. *Atmos. Environ.*, **3**, 519–536, https://doi.org/10.1016/0004-6981(69)90042-0.

Helbig, M., and Coauthors, 2021: Integrating continuous atmospheric boundary layer and tower-based flux measurements to advance understanding of land-atmosphere interactions. *Agric. For. Meteor.*, **307**, 108509, https://doi.org/10.1016/j.agrformet.2021.108509.

Helmis, C. G., Q. Wang, G. Sgouros, S. Wang, and C. Halios, 2013: Investigating the summertime low-level jet over the east coast of the U.S.A.: A case study. *Bound.-Layer Meteor.*, **149**, 259–276, https://doi.org/10.1007/s10546-013-9841-y.

Hersbach, H., and Coauthors, 2020: The ERA5 global reanalysis. *Quart. J. Roy. Meteor. Soc.*, **146**, 1999–2049, https://doi.org/10.1002/qj.3803.

Holton, J. R., 1967: The diurnal boundary layer wind oscillation above sloping terrain. *Tellus*, **19**, 200–205, https://doi.org/10.3402/tellusa.v19i2.9766.

Holtslag, A. A. M., and B. A. Boville, 1993: Local versus nonlocal boundary-layer diffusion in a global climate model. *J. Climate*, **6**, 1825–1842, https://doi.org/10.1175/1520-0442(1993)006<1825:LVNBLD>2.0.CO;2.

Hu, L., and N. A. Brunsell, 2015: A new perspective to assess the urban heat island through remotely sensed atmospheric profiles. *Remote Sens. Environ.*, **158**, 393–406, https://doi.org/10.1016/j.rse.2014.10.022.

Hu, X. M., P. M. Klein, M. Xue, J. K. Lundquist, F. Zhang, and Y. Qi, 2013: Impact of low-level jets on the nocturnal urban heat island intensity in Oklahoma City. *J. Appl. Meteor. Climatol.*, **52**, 1779–1802, https://doi.org/10.1175/JAMC-D-12-0256.1.

Imhoff, M. L., P. Zhang, R. E. Wolfe, and L. Bounoua, 2010: Remote sensing of the urban heat island effect across biomes in the continental USA. *Remote Sens. Environ.*, **114**, 504–513, https://doi.org/10.1016/j.rse.2009.10.008.

Jahn, D. E., and W. A. Gallus, 2018: Impacts of modifications to a local planetary boundary layer scheme on forecasts of the Great Plains low-level jet environment. *Wea. Forecasting*, **33**, 1109–1120, https://doi.org/10.1175/WAF-D-18-0036.1.

Jeričević, A., and B. Grisogono, 2006: The critical bulk Richardson number in urban areas: Verification and application in a numerical weather prediction model. *Tellus*, **58A**, 19–27, https://doi.org/10.1111/j.1600-0870.2006.00153.x.

Kotthaus, S., C. H. Halios, J. F. Barlow, and C. S. B. Grimmond, 2018: Volume for pollution dispersion: London's atmospheric boundary layer during ClearfLo observed with two ground-based lidar types. *Atmos. Environ.*, **190**, 401–414, https://doi.org/10.1016/j.atmosenv.2018.06.042.

Lapworth, A., 2006: The morning transition of the nocturnal boundary layer. *Bound.-Layer Meteor.*, **119**, 501–526, https://doi.org/10.1007/s10546-005-9046-0.

Liu, G., J. Sun, and W. Jiang, 2009: Observational verification of urban surface roughness parameters derived from morphological models. *Meteor. Appl.*, **16**, 205–213, https://doi.org/10.1002/met.109.

Lund, R., X. L. Wang, Q. Q. Lu, J. Reeves, C. Gallagher, and Y. Feng, 2007: Changepoint detection in periodic and autocorrelated time series. *J. Climate*, **20**, 5178–5190, https://doi.org/10.1175/JCLI4291.1.

Lundquist, J. K., and J. D. Mirocha, 2008: Interaction of nocturnal low-level jets with urban geometries as seen in Joint Urban 2003 data. *J. Appl. Meteor. Climatol.*, **47**, 44–58, https://doi.org/10.1175/2007JAMC1581.1.

Mahrt, L., 1999: Stratified atmospheric boundary layers. *Bound.-Layer Meteor.*, **90**, 375–396, https://doi.org/10.1023/A:1001765727956.

——, and D. Vickers, 2002: Contrasting vertical structures of nocturnal boundary layers. *Bound.-Layer Meteor.*, **105**, 351–363, https://doi.org/10.1023/A:1019964720989.

——, ——, and E. L Andreas, 2014: Low-level wind maxima and structure of the stably stratified boundary layer in the coastal zone. *J. Appl. Meteor. Climatol.*, **53**, 363–376, https://doi.org/10.1175/JAMC-D-13-0170.1.

Morris, C. J. G., and I. Simmonds, 2000: Associations between varying magnitudes of the urban heat island and the synoptic climatology in Melbourne, Australia. *Int. J. Climatol.*, **20**, 1931–1954, https://doi.org/10.1002/1097-0088(200012)20:15<1931::AID-JOC578>3.0.CO;2-D.

Myrup, L. O., C. E. McGinn, and R. G Flocchini, 1993: An analysis of microclimatic variation in a suburban environment. *Atmos. Environ.*, **27B**, 129–156, https://doi.org/10.1016/0957-1272(93)90001-M.

Oke, T., 1982: The energetic basis of the urban heat island. *Quart. J. Roy. Meteor. Soc.*, **108** (455), 1–24, https://doi.org/10.1002/qj.49710845502.

——, 1988: The urban energy balance. *Prog. Phys. Geogr. Earth Environ.*, **12**, 471–508, https://doi.org/10.1177/030913338801200401.

——, 1995: The heat island of the urban boundary layer: Characteristics, causes and effects. *Wind Climate in Cities*, Springer, 81–107.

Parish, T. R., and R. D. Clark, 2017: On the initiation of the 20 June 2015 Great Plains low-level jet. *J. Appl. Meteor. Climatol.*, **56**, 1883–1895, https://doi.org/10.1175/JAMC-D-16-0187.1.

——, and L. D. Oolman, 2010: On the role of sloping terrain in the forcing of the Great Plains low-level jet. *J. Atmos. Sci.*, **67**, 2690–2699, https://doi.org/10.1175/2010JAS3368.1.

Peng, S., and Coauthors, 2011: Surface urban heat island across 419 global big cities. *Environ. Sci. Technol.*, **46**, 696–703, https://doi.org/10.1021/es2030438.

Petersen, R. A., 2016: On the impact and benefits of AMDAR observations in operational forecasting. Part I: A review of the impact of automated aircraft wind and temperature reports. *Bull. Amer. Meteor. Soc.*, **97**, 585–602, https://doi.org/10.1175/BAMS-D-14-00055.1.

——, L. Cronce, R. Mamrosh, R. Baker, and P. Pauley, 2016: On the impact and future benefits of AMDAR observations in operational forecasting. Part II: Water vapor observations. *Bull. Amer. Meteor. Soc.*, **97**, 2117–2133, https://doi.org/10.1175/BAMS-D-14-00211.1.

Rahn, D. A., and C. J. Mitchell, 2016: Diurnal climatology of the boundary layer in Southern California using AMDAR temperature and wind profiles. *J. Appl. Meteor. Climatol.*, **55**, 1123–1137, https://doi.org/10.1175/JAMC-D-15-0234.1.

Reeves, J., J. Chen, X. L. Wang, R. Lund, and Q. Q. Lu, 2007: A review and comparison of change point detection techniques for climate data. *J. Appl. Meteor. Climatol.*, **46**, 900–915, https://doi.org/10.1175/JAM2493.1.

Shapiro, A., and E. Fedorovich, 2009: Nocturnal low-level jet over a shallow slope. *Acta Geophys.*, **57**, 950–980, https://doi.org/10.2478/s11600-009-0026-5.

Shibuya, R., K. Sato, and M. Nakanishi, 2014: Diurnal wind cycles forcing inertial oscillations: A latitude-dependent resonance phenomenon. *J. Atmos. Sci.*, **71**, 767–781, https://doi.org/10.1175/JAS-D-13-0124.1.

Smedman, A.-S., H. Bergström, and B. Grisogono, 1997: Evolution of stable internal boundary layers over a cold sea. *J. Geophys. Res.*, **102**, 1091–1099, https://doi.org/10.1029/96JC02782.

Smith, E. N., J. G. Gebauer, P. M. Klein, E. Fedorovich, and J. A. Gibbs, 2019: The Great Plains low-level jet during PECAN: Observed and simulated characteristics. *Mon. Wea. Rev.*, **147**, 1845–1869, https://doi.org/10.1175/MWR-D-18-0293.1.

Song, J., K. Liao, R. L. Coulter, and B. M. Lesht, 2005: Climatology of the low-level jet at the southern Great Plains atmospheric boundary layer experiments site. *J. Appl. Meteor.*, **44**, 1593–1606, https://doi.org/10.1175/JAM2294.1.

Sun, J., L. Mahrt, R. M. Banta, and Y. L. Pichugina, 2012: Turbulence regimes and turbulence intermittency in the stable boundary layer during CASES-99. *J. Atmos. Sci.*, **69**, 338–351, https://doi.org/10.1175/JAS-D-11-082.1.

Tran, H., D. Uchihama, S. Ochi, and Y. Yasuoka, 2006: Assessment with satellite data of the urban heat island effects in Asian mega cities. *Int. J. Appl. Earth Obs. Geoinf.*, **8**, 34–48, https://doi.org/10.1016/j.jag.2005.05.003.

Troen, I. B., and L. Mahrt, 1986: A simple model of the atmospheric boundary layer; sensitivity to surface evaporation. *Bound.-Layer Meteor.*, **37**, 129–148, https://doi.org/10.1007/BF00122760.

Unwin, D. J., 1980: The synoptic climatology or Birmingham's urban heat island, 1965-1974. *Weather*, **35**, 43–50, https://doi.org/10.1002/j.1477-8696.1980.tb03484.x.

Vogelezang, D. H. P., and A. A. M. Holtslag, 1996: Evaluation and model impacts of alternative boundary-layer height formulations. *Bound.-Layer Meteor.*, **81**, 245–269, https://doi.org/10.1007/BF02430331.

Wagner, T. J., and R. A. Petersen, 2021: On the performance of airborne meteorological observations against other in-situ measurements. *J. Atmos. Oceanic Technol.*, **38**, 1217–1230, https://doi.org/10.1175/JTECH-D-20-0182.1.

Wang, J., and X. M. Hu, 2021: Evaluating the performance of WRF urban schemes and PBL schemes over Dallas–Fort Worth during a dry summer and a wet summer. *J. Appl. Meteor. Climatol.*, **60**, 779–798, https://doi.org/10.1175/JAMC-D-19-0195.1.

Wei, W., H. S. Zhang, and X. X. Ye, 2014: Comparison of low-level jets along the north coast of China in summer. *J. Geophys. Res. Atmos.*, **119**, 9692–9706, https://doi.org/10.1002/2014JD021476.

Williams, S. S., T. J. Wagner, and R. A. Petersen, 2021: Examining the compatibility of aircraft moisture observations and operational radiosondes. *J. Atmos. Oceanic Technol.*, **38**, 859–872, https://doi.org/10.1175/JTECH-D-20-0053.1.

WMO, 2017: Guide to aircraft-based observations. WMO Doc. WMO-1200, 141 pp., https://library.wmo.int/doc_num.php?explnum_id=4120.

Zhang, Y., Z. Gao, D. Li, Y. Li, N. Zhang, X. Zhao, and J. Chen, 2014: On the computation of planetary boundary-layer height using the bulk Richardson number method. *Geosci. Model Dev.*, **7**, 2599–2611, https://doi.org/10.5194/gmd-7-2599-2014.

——, D. Li, Z. Lin, J. A. Santanello, and Z. Gao, 2019: Development and evaluation of a long-term data record of planetary boundary layer profiles from aircraft meteorological reports. *J. Geophys. Res. Atmos.*, **124**, 2008–2030, https://doi.org/10.1029/2018JD029529.

——, K. Sun, Z. Gao, Z. Pan, M. A. Shook, and D. Li, 2020: Diurnal climatology of planetary boundary layer height over the contiguous united states derived from AMDAR and reanalysis data. *J. Geophys. Res. Atmos.*, **125**, e2020JD032803, https://doi.org/10.1029/2020JD032803.

Zhong, S., J. D. Fast, and X. Bian, 1996: A case study of the Great Plains low-level jet using wind profiler network data and a high-resolution mesoscale model. *Mon. Wea. Rev.*, **124**, 785–806, https://doi.org/10.1175/1520-0493(1996)124<0785:ACSOTG>2.0.CO;2.

Zilitinkevich, S., and A. Baklanov, 2002: Calculation of the height of the stable boundary layer in practical applications. *Bound.-Layer Meteor.*, **105**, 389–409, https://doi.org/10.1023/A:1020376832738.